Characterization of the HeCo Mutant Mouse: A New Model of Subcortical Band Heterotopia Associated with Seizures and Behavioral Deficits

Alexandre Croquelois[1,2], Fabienne Giuliani[3,4], Christine Savary[2], Michel Kielar[2], Clotilde Amiot[5], Françoise Schenk[3,4] and Egbert Welker[2]

[1]Service de Neuropsychologie et de Neuroréhabilitation, Centre Hospitalier Universitaire Vaudois (CHUV), Avenue Pierre Decker 5, 1011 Lausanne, Switzerland, [2]Department de Biologie Cellulaire et de Morphologie, Université de Lausanne, Rue du Bugnon 9, CH-1005 Lausanne, Switzerland, [3]Institut de Physiologie, Centre de Neurosciences Psychiatriques, Site de Cery, CH-1008 Prilly, Switzerland, [4]Institut de Psychologie, Université de Lausanne, Quartier UNIL-Dorigny, Bâtiment Anthropole, 1015 Lausanne, Switzerland and [5]Service de Génétique, Histologie, Biologie du Développement et de la Reproduction (EA 3922), Hôpital Saint-Jacques, Place Saint-Jacques, 25030 Besancon cedex, France

In human, neuronal migration disorders are commonly associated with developmental delay, mental retardation, and epilepsy. We describe here a new mouse mutant that develops a heterotopic cortex (HeCo) lying in the dorsolateral hemispheric region, between the homotopic cortex (HoCo) and subcortical white matter. Cross-breeding demonstrated an autosomal recessive transmission. Birthdating studies and immunochemistry for layer-specific markers revealed that HeCo formation was due to a transit problem in the intermediate zone affecting both radially and tangentially migrating neurons. The scaffold of radial glial fibers, as well as the expression of doublecortin is not altered in the mutant. Neurons within the HeCo are generated at a late embryonic age (E18) and the superficial layers of the HoCo have a correspondingly lower cell density and layer thickness. Parvalbumin immunohistochemistry showed the presence of gamma-aminobutyric acidergic cells in the HeCo and the mutant mice have a lowered threshold for the induction of epileptic seizures. The mutant showed a developmental delay but, in contrast, memory function was relatively spared. Therefore, this unique mouse model resembles subcortical band heterotopia observed in human. This model represents a new and rare tool to better understand cortical development and to investigate future therapeutic strategies for refractory epilepsy.

Keywords: cerebral cortex growth and development, migration disorder, models: animal, neuronal neurobehavioral manifestations

Introduction

Development of the neocortex involves complex cellular and molecular mechanisms, among them neuronal genesis, migration, cell differentiation and the development of afferent and efferent connections (Rakic 1988; Honda et al. 2003). Neuronal migration is controlled by cytoskeletal molecules that regulate the initiation of migration which is subsequently controlled by a set of extracellular signaling molecules, such as the reelin pathway, and other stop signals (Gressens 2006). The morphology of pyramidal neurons undergoes several modifications that reflect the various steps in the migratory pathway (LoTurco and Bai 2006). Whereas the progenitors in the ventricular zone (VZ) are bipolar, migrating neurons are multipolar within the subventricular zone (SVZ). Upon arrival in the deep intermediate zone (IZ), they adopt a bipolar morphology, a characteristic of the migrating pyramidal neuron that is maintained until they arrive in their final position in the cerebral cortex. Interestingly, LoTurco and Bai (2006) hypothesized that failure to make the transition from the multipolar to the bipolar stage may be a characteristic of most neuronal migration disorders. Although some neocortical migrating neurons migrate almost exclusively radially, others initially take a tangential trajectory at the level of the VZ or SVZ before adopting a classical radial migration pathway (Gressens 2000). Radial migration of neurons is supported by radial glial cells (Rakic 2003) and concerns the development of cortical projection neurons, mainly glutamatergic. However, the important pool of gamma-aminobutyric acidergic (GABAergic) interneurons have their origin principally in the subcortical telencephalon, in non-primate mammals mainly in the medial ganglionic eminence (Wonders and Anderson 2005). In primates however, other sources have been proposed, including the caudal and lateral ganglionic eminences, the septal region, and the cortex itself (Wonders and Anderson 2005). Recent evidence suggests that the diversity of the origin of GABAergic interneurons can be correlated with the remarkable diversity in their differentiated state (Wonders and Anderson 2005).

In human, neuronal migration disorders form a group of brain malformations which primarily affect development of the cerebral cortex (Dobyns and Truwit 1995). They are mainly caused by genetic alterations (Clark 2004, for review). Other etiologies are infections during pregnancy as well as ischemic and toxic insults. Such alterations are likely to affect neuronal migration to the cortex during the third and fourth months of gestation (Dobyns and Truwit 1995). However, currently evidence exists that other pathogenic mechanisms could cause subcortical accumulation of neurons such as modified cellular proliferation and programmed cell death (Clark 2004). Neuronal migration disorders range in severity from minor displacements of a few neurons (Meencke and Veith 1999; Eriksson et al. 2005) to massive rearrangements of cortical structure including the formation of subcortical heterotopia, also called double cortex. This severe form of diffuse subcortical heterotopia is commonly associated with a delay in somatic development, mental retardation, and epilepsy. The incidence of cortical malformations is more than 1% in the human population. Fourteen percent of epileptic patients have a cortical malformation based on a migration disorder. This incidence rises to 40% in patients with intractable epilepsy, the majority of them already presenting seizures during infancy (Farrell et al. 1992; Meencke and Veith 1992; Guerrini 2005).

We here characterize the phenotype of a new and unique genetic mouse model of cortical heterotopia (the HeCo

[heterotopic cortex] mouse). The mutation appeared spontaneously in our colony of the NOR strain derived from ICR-stock (Van der Loos et al. 1986) and was discovered during an unrelated experiment (Croquelois et al. 2005). We identify and characterize here the cortical malformation, its mode of inheritance and its developmental schedule, as well as the associated neurological and behavioral deficits exhibited by HeCo mutant mice.

Materials and Methods

Mice of the NOR and C57/Black6 (C57/Bl6) strains were used in this study. All the procedures described beneath were reviewed and approved by the Office Vétérinaire Cantonal (Lausanne, Switzerland), following Swiss Federal Laws.

Cross-Breeding Experiments

The first HeCo mouse was discovered using histological brain sections performed for unrelated experiments. Selective inbreeding including crossing of living relatives and backcrossing were used to increase the occurrence of the phenotype in offspring. Crossings of HeCo females with C57/Bl6 unaffected males and of HeCo males with C57/Bl6 unaffected females were then performed to define the transmission mode. Phenotype was determined in Nissl-stained coronal sections throughout the forebrain.

BrdU Injections and Immunohistochemistry

Mutant and control pregnant females were injected intraperitoneally with 5-bromo-2′-deoxyuridine (BrdU) (100 μg/g body weight, in phosphate buffered saline [PBS] 0.1 M, Sigma, St Louis, MO). Injections were performed at either embryonic (E)13 (brain removal at postnatal [P]13), E14 (brain removal at E15), E15 (brain removal at E16 and P13), E16 (brain removal at E17), or E18 (brain removal at P13) stages. The day of vaginal plug detection was designated as day 0 of gestation (E0). For juvenile animals (brain removal at P6 or P13), mice received a lethal dose of pentobarbital and were immediately fixed via cardiac perfusion with a solution of paraformaldehyde (1% in phosphate buffer 0.1 M, pH 7.4, for 5 min, then 4% in phosphate buffer 0.1 M, pH 7.4, for another 10 min). For embryos, brains were removed and immersed in paraformaldehyde (4% in phosphate buffer 0.1 M, pH 7.4) for 4 h. After cryoprotection in sucrose (30% overnight), brains were serially cut at 40-μm thickness using a sliding cryotome. Alternate sections were either stained with Cresyl Violet, processed for BrdU immunohistochemistry or immunohistochemistry for Cux-2, Tbr1, RC2, GLAST, and Dcx (doublecortin). For Parvalbumin (PARV)–immunohistochemistry we used 4 adult HeCo mice that were not exposed to BrdU.

BrdU Immunohistochemistry

We used the protocol described by Takahashi et al. (1992). In brief, sections were immersed in 2 N HCl for 60 min, neutralized in tris-buffered saline (TBS) for 3 × 10 min, and then incubated with primary antibody (anti-BrdU, mouse monoclonal, clone Bu20a, Dako, Switzerland) at a dilution of 1:100 in TBS 0.05 M overnight at 4 °C. Sections were rinsed in TBS and incubated in biotinylated secondary antibody (Biotin-SP-conjugated AffiniPure Goat Anti-Mouse, Jackson Immuno-Research Europe, Newmarket, UK) for 60 min. The sections were then processed with avidin-biotin-peroxidase complex (ABC) (Vector Laboratories, Peterborough, UK) for 60 min, rinsed in PBS, and visualized with diaminobenzidine (DAB) (Sigma). Sections were dehydrated in a series of graded ethanols, cleared in xylene, and coverslipped using Permount.

Immunohistochemistry

PARV Immunohistochemistry

Sections were thoroughly rinsed in PBS, and incubated in a blocking solution containing 10% normal goat serum and 4% bovine serum albumin in PBST (0.2% Triton X-100 in PBS) for 1 h at room temperature. After rinsing, sections were incubated overnight at 4 °C with rabbit anti-PARV (1:1000) antibody. Thereafter, sections were

sequentially incubated with biotinylated goat anti-rabbit antibodies (1:200) and with the ABC (1:200). Peroxidase was developed with 0.05% diaminobenzidine in 0.1 M PB and 0.005% hydrogen peroxide. Thereafter, immunoreacted sections were mounted onto gelatinized slides.

Tbr-1, Cux-2, RC2, GLAST, Dcx Immunohistochemistry

Sections were blocked with 2% normal horse serum in PBST with azide (phosphate buffer 0.1 M, NaCl 0.9%, Triton 0.3%, Azide 1 g/L; blocking solution) then incubated overnight at 4 °C with primary antibodies diluted in blocking solution. Secondary antibodies diluted in PBS 0.9% with Triton 0.3% were applied for one hour. Sections were then rinsed in PBS, mounted with chrom-alun 4% and coverslipped. Primary antibodies used: anti-Cux-2 (Millipore Corporation) at 1:150, anti-Tbr-1 (Millipore AG, Zug, Switzerland) at 1:1000, anti-RC2 (Developmental Studies Hybridoma Bank, University of Iowa) at 1:200, anti-GLAST (Millipore Corporation) at 1:5000 and anti-Dcx (Santa Cruz Biotechnology, Santa Cruz, CA) at 1:100, all raised in rabbits. Secondary antibodies used: Alexa 488 Donkey anti-Rabbit (Invitrogen) at 1:300 for Cux-2 and GLAST and Alexa 594 Donkey anti-Rabbit (Invitrogen) at 1:300 for Tbr-1, RC2, and Dcx.

Reconstruction and Morphometric Analysis

To morphometrically characterize the neurons of the HeCo and those of the overlying homotopic cortex (HoCo), contours of neuronal cell body were drawn with a computer controlled microscope and the Neurolucida Software (Microbrightfield, Magdeburg, Germany) in 4 consecutive Nissl-stained sections (spaced 80 μm from each other on the rostro-caudal axis) in both control ($n = 4$) and mutant ($n = 4$) mice. The most rostral section was taken at the level of the most rostral part of the hippocampal formation. Radial thickness of the HeCo and the cortical layers of the HoCo together with cell density were also recorded.

BrdU-positive cells in the cerebral cortex of the right hemisphere were quantitatively analyzed using the brains of 3 P13 mice for each injection date (E13, E15, and E18). Positive cells were plotted using the same device. Per brain, 3 sections (spaced 80 μm from each other on the rostro-caudal axis) were analyzed. The most rostral section was taken at the level of the most rostral part of the hippocampal formation. In mutant mice, 3 contours were drawn around the HeCo, the HoCo and the adjacent, more lateral, cortex (AdCo). In control mice contours corresponding to the HoCo and the AdCo as determined by distance to midline were also drawn. To define the relative position of BrdU-positive neurons within these different regions of interest, the position of the subcortical white matter was plotted for the HeCo and the AdCo. For the HoCo, the thin band of white matter lying between the HeCo and the HoCo was identified as well. These reference lines were used to extrapolate the different curves using Lagrange interpolating polynomial. Migration distance was defined for each cell by the minimal distance to the corresponding curve. To allow comparison of the number of BrdU-positive cells between the 3 regions of interest and across embryonic ages of BrdU injection, we divided each region of interest in 10 equivalent tangentially oriented stripes, stripe 1 being the deeper and stripe 10 the more superficial one. The mean number of positive cells for each stripe was obtained from the 4 sections of the 4 animals in each group.

PARV+ cells in the cerebral cortex of the right hemisphere were plotted using the brains of the 4 mutant mice in the same way. Cells were plotted in 3 different regions of interest: the HeCo, the HoCo, and the AdCo. The number of PARV+ cells per surface unit, cell size and distance to the closest PARV+ cell were determined.

Tracing Experiments

To study neuronal connectivity of the HeCo, 3 mutant mice were anaesthetized with pentobarbital (sodium pentobarbital 60 mg/kg body weight i.p.) and placed in a stereotaxic frame. Part of the skull overlying the medio-dorsal cortex was removed and the HeCo was identified using extracellular recording and stereotaxic coordinates. Biotinylated dextran amine (BDA, Molecular Probes D-7135, MW 3000, Eugene, OR) was injected into the HeCo. The pressure injection was made at 1000-μm cortical depth and lasted for 2 min using the following parameters: 70 nL of a 5% solution in PBS (phosphate buffer 0.1 M, 0.9% saline, pH 7.4). After 10 days survival time, the animals were deeply anaesthetized and

perfused with paraformaldehyde (4% in 0.1 M phosphate buffer, pH 7.4). Serial coronal sections were cut at 40-μm thickness. Sections were processed for DAB reaction (Veenman et al. 1992) and counterstained with toluidine blue.

Histological Examination of Organs and Blood Tests

Adult mice (4 HeCo and 4 controls) received a lethal dose of pentobarbital and were immediately fixed via cardiac perfusion with a solution of paraformaldehyde (4% in phosphate buffer 0.1 M, pH 7.4, for 15 min). Following cryoprotection in 30% sucrose overnight, heart, liver, pancreas, spleen and kidney were removed and cut at 40-μm thickness with a cryotome. Sections were stained with hematoxylin–eosin. Blood samples from 4 control and 4 HeCo mice were obtained after a 16-h fasting period and processed for analysis of electrolytes (Na^+, K^+, Cl^-), creatinin, glucose and cholesterol.

Pilocarpine Induced Status Epilepticus

Sensitivity for the development of epileptic seizures was compared between HeCo and control mice using the pilocarpine induced status epilepticus (SE) model (Cavalheiro et al. 1996). Seventeen mice (12–16 weeks of age) received an intraperitoneal injection (i.p.) of methyl-scopolamine at a dose of 1 mg/kg body weight 30 min prior to injection of pilocarpine to reduce its peripheral cholinergic effects. Animals were then intraperitoneally injected with a single dose of either 100 or 200 mg/kg of pilocarpine in 0.2-mL sterile saline vehicle (0.9% NaCl). Animals were observed continuously and epileptic seizures and/or SE were recorded. Mice that developed a SE were deeply anesthetized with sodium pentobarbital (60 mg/kg body weight i.p.) and subsequently perfused with paraformaldehyde (4% in phosphate buffer 0.1 M, pH 7.4). Coronal sections were cut at 40-μm thickness and processed for Nissl staining.

Behavioral Experiments

A total of 92 mice were used, 23 HeCo and 35 control mice from P0 to P22, 5 HeCo and 5 control mice at the age of 2 months and finally 9 HeCo and 15 control mice aged more than 7 months. Behavior was analyzed in different situations in order to assess the early development of locomotor capacities and complementary aspects of potential cognitive deficits linked to the HeCo phenotype.

Two spatial tasks were adapted, the Morris navigation task and the 8-arm radial maze. In addition, one set-up was designed to assess locomotor activity (Grandchamp and Schenk 2006).

The early development of locomotion was assessed in 2 conditions. Contact righting was observed on a rough substrate of 25 × 20 cm, limited on 3 sides by a 5 cm high wall. Negative geotaxis capacity was recorded on a rough substrate (25 × 20 cm). Its surface was tilted 25° from the horizontal plane. The infant mouse was able to clutch the rough surface and was also prevented from passive slipping due to the enhanced friction.

The Y-maze was composed of 3 (6 × 6 × 50 cm) transparent Plexiglas runways (named A, B, and C) linked together in a symmetrical Y shape (120° of angular deviation from each other). The olfactory automated radial maze was made of 8 transparent Plexiglas tunnels (6 × 6 × 50 cm) placed on a circular table covered by a plastic sheet. Three arms were baited with a drop of diluted condensed milk deposited on a glass plate at the end of the tunnels. The olfactory cues were bands of blotting paper (2 × 50 cm) affixed to the arms' ceiling. The cues were made by impregnating the blotting paper bands with 0.8 mL of solutions made with 8 different alimentary aromas (lemon, apricot, aniseed, orange, blackcurrant, apple, amend bitter, brandy). Guillotine doors closed the exit of each tunnel.

The Morris navigation task was performed using a circular pool (120 cm in diameter, 30 cm height) made of gray polyvinyl chloride that was situated in a dimly illuminated room. The pool was filled to a depth of 15 cm with water (27 °C) opacified with milk (0.5 L). Four orthogonal starting positions around the perimeter of the pool, divided its surface into 4 quadrants. A platform consisting of a transparent Plexiglas cylinder (15 cm tall and 8 cm diameter) and covered with a white aluminum perforated plate (14 cm diameter) was placed in the center of the quadrants, approximately 0.5 cm under water level. The pool was located in a room containing numerous extra-maze cues.

Morphologic and motor developments were evaluated as follows. Body weight and hair growth was assessed daily. Time of eye opening was recorded for each mouse. The locomotor development included a description of locomotion strategies, the assessment of contact righting and negative geotaxis. Spontaneous locomotion was recorded daily during 2 min on a horizontal plan according to 5 items described by Altman and Sudarshan (1975), pivoting (the front legs push like paddles and the rear wheel-axle unit is practically motionless), punting (the head is posed over a leg, the leg is withdrawn and placed in the direction of the movement while the other leg pushes to help it), treading (the head is elevated, the movements of the front legs are not more constrained; at the same time, the posterior legs are more isolated and offer a better support), crawling (the belly rests by ground but the posterior legs become mobile) and walking (the belly does not touch any more by ground and there is a synchronization of the legs).

For the negative geotaxis test, the animal was deposited with the head oriented downwards, in the center of the tilted plan. The test lasted a maximum of 3 min and the position of the animal was recorded every 5 s with a precision of 15°, from the starting position (–90°), through the horizontal plan (0°) to the expected position with the head upwards (+90°). The test started at day 5 and was prolonged until the animal tried to escape from the apparatus.

To test general activity, mice were individually placed in the distal end of an arm of the Y-maze for 8 min free exploration. The starting position for each mouse was randomly A, B, or C runway. Two kinds of measures were recorded. First, the number of arm entries as an indication of general activity. Second, alternation behavior was assessed from the individual sequences of arm visits. The frequency of 3-arm alternations (ABC-type) was compared with the frequency of incomplete or null alternation patterns (ABA-, BAA-, or AAA-type). For the 20- and 22-day-old mice, a black cue was placed opposite the arm B.

Cognitive tasks were tested using the automated radial maze and the Morris water maze. Mice were trained over 9 consecutive daily sessions in an automated 8-arm radial maze to discriminate the 3 arms that were constantly baited with food and the 5 arms that were never baited. A first exploration session consisted of leaving each mouse during 10 min in the maze with free access to all the tunnels and with all arms baited with food to familiarize them with the maze and its environment. After that, the animals received 6 daily learning trials. Two different configurations of 3 baited arms were used, always the same for a given mouse throughout training. The baited and non baited arms were thus at fixed positions in space and could also be discriminated by a specific odor cue. An arm was baited or non baited depending on the test subject so that no particular arm could accumulate scent marks due to the presence or absence of reinforcement. Each subject was assigned a different set of 3 constantly baited arms (arms 1, 4, 6 or 2, 5, 7) with the sequence of angles between the baited arms being 135°–90°–135°. Mice were individually introduced into the central platform and each trial started by the opening of all 8 doors simultaneously. After each visit to an arm, the door giving access to that arm was automatically closed, preventing re-entries into an already visited arm. Each trial was terminated after the animal retrieved the third food pellet and had returned to the central platform; all 8 doors were closed simultaneously and the animal was left 1 min in the central platform. During the entire testing period, all the mice had restricted access to food and their weight was checked every day to prevent more than a 10% body weight loss. Discrimination performance was assessed by the mean of total errors for each trial (with a maximum of 5 errors) calculated for each day.

For the Morris water maze task, the mice received 4 daily learning trials during 5 days. The position of the hidden platform remained fixed for the entire period of the acquisition and each subject was assigned a different sector. Each trial started with the mice being placed into the water, at one of 4 starting points: N, E, S, W. Four different starting positions were pseudorandomly used in each training block. A trial ended when the mouse reached the hidden platform and it was allowed to remain there for 20 s. If a successful escape was not performed within 60 s, the mouse was guided to the platform and the trial was recorded as an escape failure. Between successive trials the test mouse

was left for a 30-s intertrial interval in a dry container. Each mouse was dried in the container with cellulose paper before being replaced in its home cage. At the end of the 20 training trials, each mouse received a probe trial. For this trial, the platform was removed from the pool and the mouse was allowed to swim for 60 s. Then the platform was replaced in the training location and the mouse was allowed to climb on it. For the learning and transfer stages, a variable was measured: the average number of errors across all days to find the platform (% errors). For the probe trials, we compared the time spent in the training half of the pool (containing the platform during training) with the opposite one.

For all the experiments, a video camera suspended directly above each apparatus was connected to a computer and used to record the mice behavior. Experiments took place during the light phase between 7:00 a.m. and 7:00 p.m.

Statistics

The statistical analysis was performed using the SAS package (SAS Institute Inc., Cary, NC) and StatView (version 4.5). Data were checked for the normality of distribution. Comparisons of means in 2 groups were made using the unpaired Student's t-test. When comparison was based on the means of more than 2 groups we applied an analysis of variance (ANOVA). For the BrdU study, data related to the different stripes defined above were analyzed with the multivariate ANOVA using the generalized linear model procedure. For the behavioral experiments, ANOVAs were performed on the raw data with the genotype as the between-subjects and repeated measures such as day, session, area,

as within-subject factors. The ANOVAs were confirmed by unpaired t-test and other pair comparisons were performed by a post hoc test (Fisher post-hoc least significant difference, $P < 0.05$), when necessary. Parametric correlations (r) and Spearman rank correlation were computed. The limit of significance, if unspecified, was $P < 0.05$ for all tests.

Results

HeCo Morphology

The HeCo phenotype is defined by the presence of a subcortical band heterotopia, that is located bilaterally beneath the medial part of the neocortex and extends from the frontal lobe to the occipital lobe (see Fig. 1A,B). The HeCo is separated from the overlying neocortex (HoCo) by a thin layer of white matter, and from subcortical structures by a thicker layer of white matter, resembling normal subcortical white matter. Even though the medio-lateral as well as the rostro-caudal extension of the cortical heterotopia varies between animals (for comparison see Fig. 1A,B), its general appearance and location is constant. Interestingly, notable differences in severity were identified between animals of the same offspring and, to a lesser extent, between hemispheres of the same animal. Underlying subcortical structures, including the hippocampus, striatum and thalamus as well as the cerebellum and brainstem have
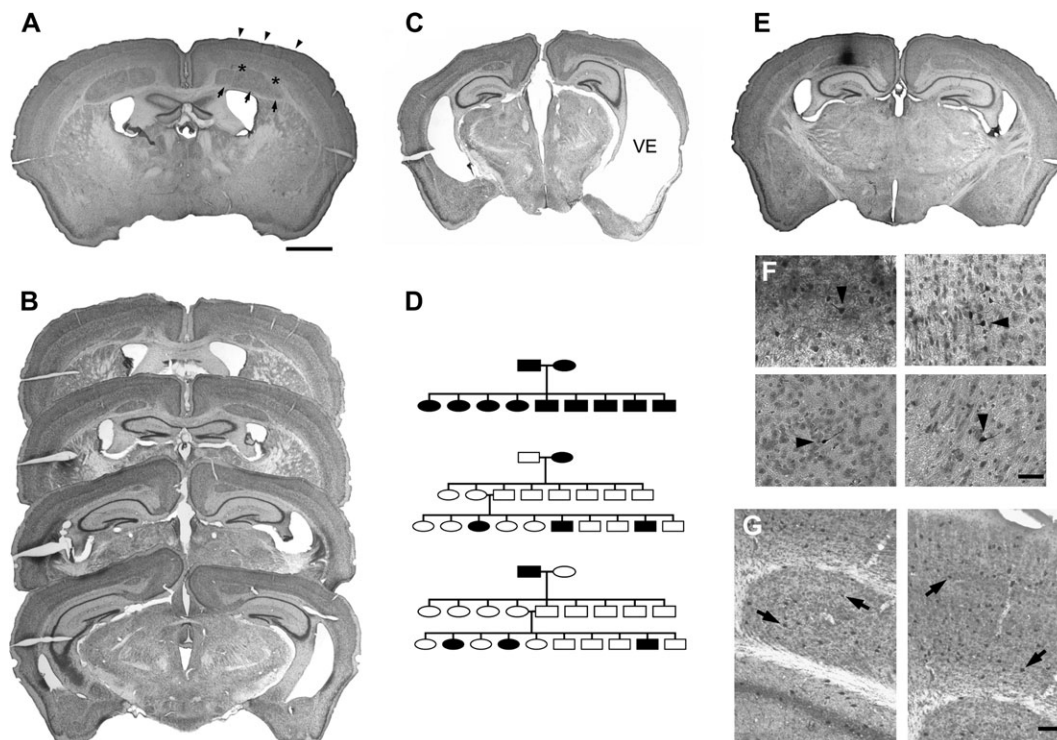

Figure 1. (*A*) Nissl-stained coronal section from a HeCo mouse. Arrows point to HeCo, asterisks to subcortical white matter and arrowheads to HoCo. (*B*) Photomicrograph of 4 consecutive Nissl-stained coronal sections of a HeCo mouse brain from rostral to caudal, showing the antero-posterior extension of the cortical heterotopia. (*C*) Photomicrograph of a coronal section of a HeCo mouse brain with severe lateral cortical atrophy and subsequent ventricular enlargement (VE). (*D*) Pedigree of different crossings between HeCo and control animals. Crossings between 2 affected mice (15 breeding pairs) revealed a 100% positive HeCo phenotype in offspring ($n = 110$). Results of the crossing of a HeCo female (black oval) with a C57/BL6 unaffected male (open square) and F2 generation from this offspring, with subsequently the reverse crossing with a HeCo male (black square) with a C57/BL6 unaffected female (open oval). Note that in either of these cases none of the F1 offspring had the HeCo phenotype, excluding a dominant or sex-linked trait. The frequency of affected mice in the F2 generation of the 2 crossings (60/247 and 10/47, respectively) indicates that the HeCo phenotype is due to an autosomal recessive disorder of a single locus. (*E* and *F*) Results of BDA-tracing in a HeCo mouse. (*E*) Photomicrograph at low power of a coronal section counterstained for Nissl-substance. Note the injection site located in the HeCo in the right hemisphere. (*F*) Photomicrographs at higher magnification showing cell labeling (black arrowheads) in the ipsilateral HeCo (upper left), the ipsilateral HoCo (upper right), the contralateral HeCo (lower left) and the ipsilateral thalamus (lower right). (*G*) Results of immunochemistry for PARV in an experimental mouse. Photomicrographs at high magnification showing the ipsilateral HeCo (left) and the ipsilateral HoCo (right). Black arrows indicate PARV+ cells. Scale bars: (*A–D*) 1000 μm, (*E*) 50 μm, (*F*) 100 μm.

a normal microscopic appearance but a discrete ventricular enlargement is observed as compared with mice of the NOR strain that do not display the HeCo phenotype. In a small number of animals, a more severe malformation was present with a lateral cortical atrophy and huge ventricular enlargement (see Fig. 1C). During general animal inspection, HeCo and control mice are hard to distinguish, except for these more severe cases where mice are small and have a low body weight with sometimes a cranial malformation and brady- and hypokinesia. Other organs, including the heart, liver, pancreas, spleen and kidney have a normal microscopic appearance and no differences were found in the serum levels of electrolytes (Na^+, K^+, Cl^-), creatinin, glucose and cholesterol between HeCo and control age and sex matched mice (results not shown).

Cross-Breeding Experiments

In these experiments the phenotype was determined in histological sections through the forebrain taken after the adult mouse had given off-spring. Crossings between 2 affected mice (15 breeding pairs) revealed a 100% positive HeCo phenotype in offspring ($n = 110$). Crossings between affected HeCo mice and unaffected C57/Bl6 mice (10 breeding pairs) revealed no HeCo-phenotypes in the offspring ($n = 78$ for all crossings, $n = 56$ for crossings between C57/Bl6 male and HeCo female, $n = 22$ for crossings between HeCo male and C57/Bl6 female). These results exclude a dominant or sex-linked trait. F2 generations from these crossings between HeCo and C57/Bl6 mice demonstrated that 70 out of 294 mice (24%) were affected which exclude a multiloci origin and demonstrate the autosomal recessive nature of the HeCo phenotype (see Fig. 1D).

Tracing Experiments

After BDA injections in the HeCo of the right hemisphere, retrogradely labeled cells were found in the HoCo, in the contralateral HeCo and HoCo and in the ipsilateral thalamus (see Fig. 1E,F). Afferent connections to the HeCo are therefore comparable to connections of the HoCo.

PARV Immunostaining

PARV+ cells were found in the HoCo, in the hippocampus, in subcortical structures as well as in the HeCo, demonstrating the presence of GABA cells in the cortical heterotopia (see Fig. 1G). Density (60, 63, 65 [cells/mm^2]) and distribution, defined by the mean distance to the closest positive cell (65, 64, 65 [μm]) of PARV+ cells were not significantly different in the HeCo, HoCo, and the adjacent cortex (AdCo), respectively. It has to be noted that this analysis does not take into account the absence of layering in the HeCo and the layer-dependent density differences in the HoCo and AdCo.

Morphometric Analysis

The thickness of the HoCo is slightly smaller in the HeCo mouse compared with cortical thickness in the control (Fig. 2A), but this difference did not reach significance. However, the HeCo together with the HoCo gives a total cortical thickness that is larger in HeCo than in control mice (Mann–Whitney test, $P < 0.0001$). To determine if all layers of the HoCo are equally affected, we compared individual layer thickness with its corresponding cortical layer in control mice. Figure 2B displays the results of this analysis showing that the only significantly affected layer is layer II/III (Mann–Whitney

test, $P = 0.0003$). We completed this morphometric investigation of the various cortical layers by determining the cell density in each layers (Fig. 2C). Analysis revealed that the cell density in layer II/III of the HeCo was significantly lower than in controls (Mann–Whitney test, $P = 0.0275$). Finally, we made a comparison of cell size between the heterotopia and layer II/III and observed that there was no significant difference in cell size between both regions (Fig. 2D).

Cell Markers

Immunolabeling by anti-Cux-2 (a marker of supragranular and granular layers) and anti-Tbr-1 (a marker of infragranular layers) antibodies are shown in Figure 3. The Tbr-1 antibody strongly labels cells in the deep cortical layers of both the normal cortex of control mice and the HoCo of mutant mice, with no cell labeling within the HeCo. Intense cell labeling by anti-Cux-2 antibodies was noted in superficial cortical layers in both the normal cortex of control mice and the HoCo of mutant mice, but this antibody also labeled virtually all the cells that form the HeCo.

Analysis of the Birth Dates of Cells in Heco, HoCo, and AdCo

At P13, BrdU-positive cells were present in infragranular, granular and supragranular layers of the HoCo and AdCo when the BrdU injection took place at E13, E15, and E18, respectively (see Fig. 4A). We found very few BrdU-positive cells in the HeCo after injection at E13 and E15. However, BrdU injection at E18 revealed a large number of positive cells in the HeCo (see Fig. 4A).

The quantitative analysis of the number of BrdU-positive cells in the HeCo demonstrated that this number was significantly different between embryonic ages of injection (multivariate ANOVA [MANOVA], $P < 0.0001$). Univariate comparisons revealed that the number of positive cells in the HeCo was higher for the E18 injection group than for E13 and E15 injection groups. No statistical differences were found between the 10 analyzed stripes in the HeCo (see Fig. 4B).

Analyzing data from the HoCo and AdCo revealed that HeCo formation disrupts the formation of the overlying cerebral cortex. MANOVA indicated that the number of BrdU-positive cells in the HoCo was significantly different between HeCo and control mice with an important drop in the number of labeled cells in the superficial stripes in HeCo mice ($P < 0.05$, see Fig. 4C). The same analysis in the AdCo also showed a less pronounced but significant drop in the number of labeled cells in the superficial stripes (see Fig. 4D).

Development of the Cerebral Cortex and Heterotopia

Histology of coronal sections at E16, 17, and 19 revealed an increase in the IZ thickness in HeCo mice compared with control animals, with a high cell density area beneath the subplate, and therefore within the IZ (see Fig. 5A). At P0, the size and extent of the cortical heterotopia was very similar to that observed in adult animals (see Fig. 5B). Results of immunochemistry for Tbr-1 at E17 and E19 confirmed this increase of the IZ and demonstrated a wider distribution of positive cells within this zone (see Fig. 6A) in HeCo mice. BrdU immunochemistry also revealed a wider distribution of positive cells within the IZ in HeCo animals (see Fig. 6B). Finally, immunochemistry for RC2 and GLAST (here used as marker for the radial glia) and Dcx showed no obvious differences

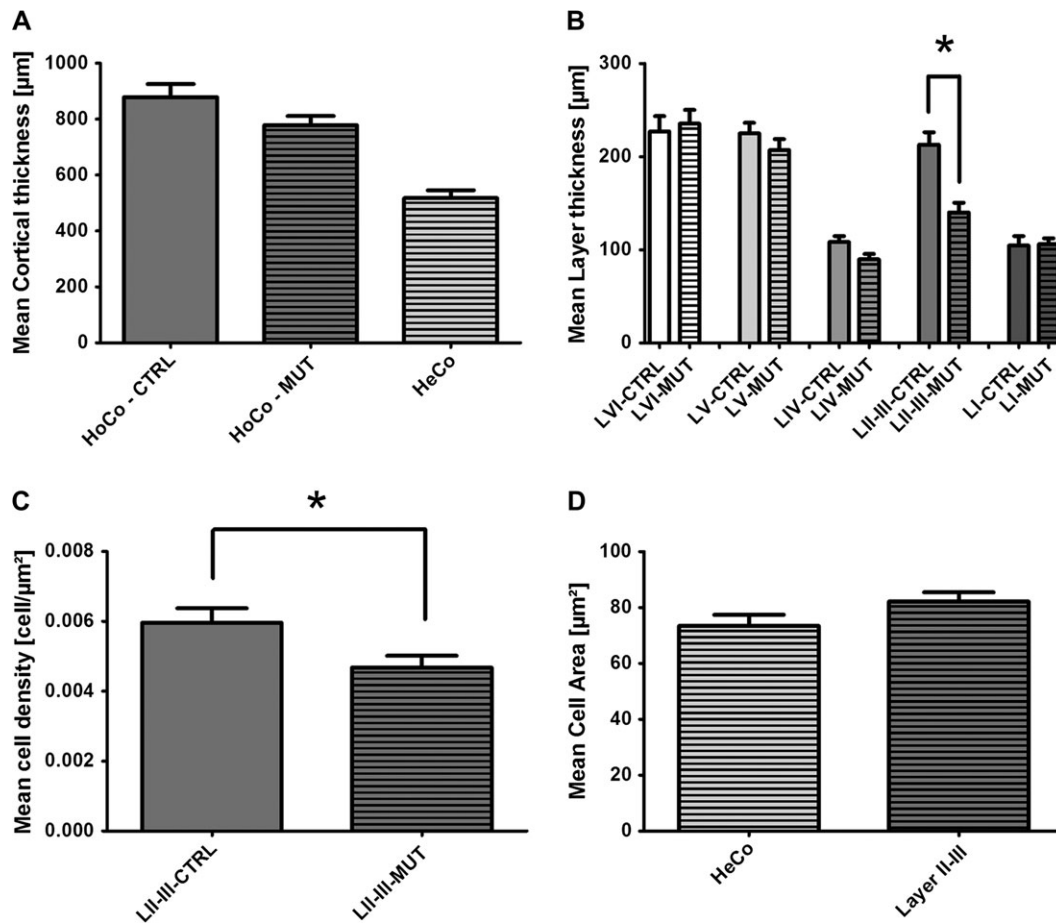**Figure 2.** Results of the morphometric analysis. (*A*) Mean thickness (±SD) of the normal cortex in control animals (HoCo—CTRL, $n = 16$), and the HoCo (HoCo—MUT) and the radial extent of the heterotopia (HeCo—MUT) in mutant mice ($n = 16$). A slight, non significant, decrease in HoCo thickness was observed in mutant mice. (*B*) Comparison of the mean layer thickness within the HoCo of both the control (CTRL, $n = 16$) and mutant (MUT, $n = 16$) mice. Note that a significant decrease in layer thickness was only observed for layers II–III of the HoCo of both the control and HeCo mice. A significant decrease in cell density was observed in mutant animals. (*D*) Comparison of cell size (here represented by cell area) between the heterotopia (HeCo) and layers II–III of the HoCo of mutant animals; no significant differences were detected.

between control and HeCo mice at E15 and confirmed the increase in IZ thickness in HeCo mice at E17 (see Fig. 7).

Spontaneous Seizures

At 8–12 weeks of age, no epileptic seizures were observed during the 24-h video recording period ($n = 24$). In younger animals (4–5 weeks of age), spontaneous myoclonic jerks associated with interruption in exploratory behavior were observed in all of the 23 HeCo animals, but never in control age matched animals ($n = 35$). In 3 out of the 23 HeCo animals spontaneous seizures similar to pilocarpine induced seizures (see below) occurred after behavioral experiments. This never occurred in age matched controls ($n = 35$).

Pilocarpine Induced SE

Compared with wild-type animals, the HeCo mice showed a significant increase in tendency to develop epileptic seizures in the pilocarpine-induced model of epilepsy. In this model, a SE is obtained at a dose of 300–350 mg/kg body weight (Cavalheiro et al. 1996). When injected with a dose of 100 mg/kg body weight, none of the 4 mutants tested developed a SE. On the other hand, all the 9 HeCo mice developed a SE when injected with the dose of 200 mg/kg body weight, whereas none of the 4 control mice did with the same dose.

Behavioral Experiments

The results of the tests for somatic growth and sensorimotor activity are presented in Figures 8 and 9. The mice of the 2 genotypes do not differ in growth rate (see Fig. 8*A*). Despite their apparently normal growth rate, the HeCo showed a significant delay in hair growth (see Fig. 8*B*) and eye opening (see Fig. 8*C*). Separate one-way ANOVAs revealed significant effects of genotype on hair growth ($F_{1,34} = 25.850$, $P < 0.0001$) and eye opening ($F_{1,34} = 7.855$, $P = 0.0083$).

The slower development of locomotion in some of the HeCo mice is illustrated in Figures 8*D* and 9. In fact, all of the control mice ($n = 35$) displayed a normal locomotion pattern at the age of 10 days, whereas only 14 of 23 HeCo mice reached the same criterion. This was related to a one-day delay in the development of efficient righting response and to a more marked delay in geotaxis reflexes (see Fig. 8*E,F*). The behavior in sensorimotor tests was significantly correlated with the development of walking. Individual results for the righting test (see Fig. 9) were correlated with the onset of walking ($r = 0.669$, $P < 0.0001$) and the response in negative geotaxis tested at 9 days ($r = 0.278$, $P = 0.0343$). These analyses were confirmed by Spearman rank correlations.

General activity assessed by the Y-Maze was significantly different between control and HeCo mice, but this difference
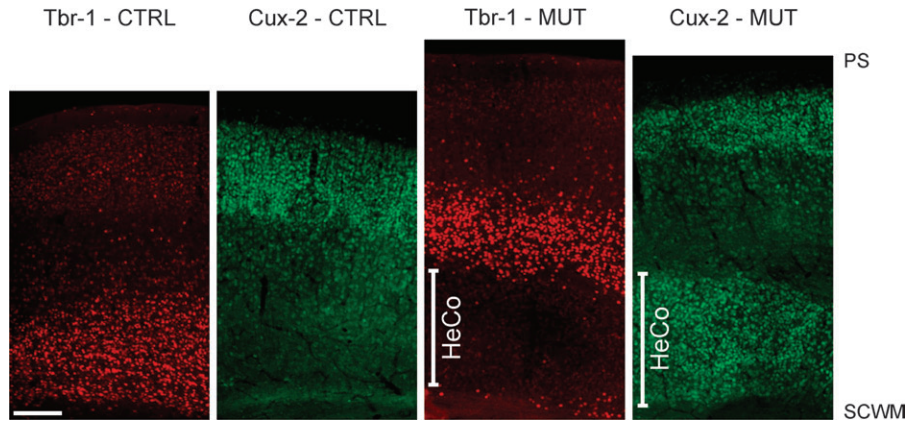
Figure 3. Results of immunohistochemistry for Tbr-1 and Cux-2 at P6. Note the strong cell labeling of deep cortical layers by anti-Tbr-1 antibody in both the normal cortex of the control (CTRL) mouse and the HoCo of the mutant (MUT) mouse, with almost no cell labeling of the HeCo. Intense cell labeling by anti-Cux-2 antibody is observed in superficial cortical layers in both the normal cortex of the control mouse and the HoCo of the HeCo mouse but also in the HeCo. Scale bar represents 200 μm. SCWM: Subcortical white matter, PS: pial surface.

Figure 4. Results of immunochemistry for BrdU injected at embryonic day 13 (E13) 15 (E15) and 18 (E18) in both control (CTRL) and mutant (MUT) mice. (*A*) Photomicrographs at low magnification showing after injection at E13 labeling in lower layers in both control mice and HoCo of mutant mice with almost no labeling in HeCo; after injection at E15, labeling in intermediate layers in both control mice and HoCo of mutant mice with again almost no labeling in HeCo; and, after injection at E18, labeling in upper layers in both control mice and HoCo of mutant mice, together with intense labeling in the HeCo. (*B–D*) Line graphs of BrdU analysis. (*B*) Comparison of the number of labeled cells in HeCo between animals of the 3 injection time groups, embryonic age 13 (E13), 15 (E15), and 18 (E18) and determined at P13. Note the relatively low number of cells at E13 and E15 and the important number of labeled cells when the injection took place at E18. (*C*) Comparison of the number of labeled cells in the HoCo in mutant (MUT) and control (CTRL) mice when the injection was performed at E18 with determination at P13. Note the important drop in labeled cells in the superficial part in the HoCo of mutant mice. (*D*) Comparison of the number of labeled cells in AdCo in mutant mice and control animals when the injection was performed at E18 with determination at P13. Note the significant drop in labeled cells in the superficial stripes in mutant mice.
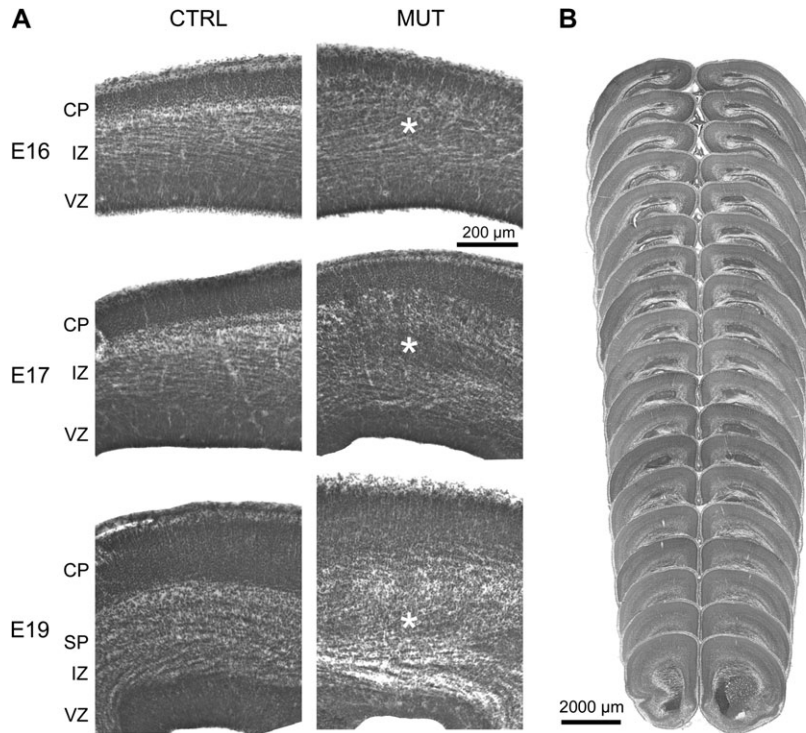
Figure 5. (*A*) Photomicrographs of coronal Nissl-stained sections through the developing cerebral cortex of control (CTRL) and mutant (MUT) mice at embryonic age 16 (E16), 17 (E17), and 19 (E19). Note the increase in IZ thickness in HeCo mice at all ages with normal thickness of the VZ and the cortical plate (CP) as compared with the control animals. Asterisks highlight a condensation of cell bodies within the IZ in HeCo mice, which is already present at E16. (*B*) Photomicrographs of consecutive coronal sections through the forebrain of a new born HeCo mouse. Note the presence of the cortical heterotopia throughout the antero-posterior axis, which is very similar to the observed heterotopia distribution in adults.

was only observed at the age of 2 months (see Fig. A in Supplemental Data). This was confirmed by a 2-way ANOVA (4 ages × 2 genotypes) revealing a significant effect of age ($F_{3,28}$ = 68.017, P < 0.0001) but not of genotype, and a significant interaction between age and genotype ($F_{3,84}$ = 8.674, P < 0.0001). Unpaired T-tests revealed a significant effect of genotype at 2 months only (P = 0.0191). The frequency of complete alternations (e.g., ABC pattern vs. ABA, BAA, or AAA) was lower in the HeCo than in control mice at 20 days only (see Fig. A in supplemental data). This was confirmed by a 2-way ANOVA (4 ages × 2 genotypes) revealing a significant effect of age ($F_{3,28}$ = 6.342, P = 0.0006) but not of genotype, and a significant interaction between age and genotype ($F_{3,84}$ = 2.913, P = 0.0391). Unpaired T-tests revealed a significant effect of genotype at 20 days only (P = 0.0044). Arm selection analyzed on the combined 20- and 22-day-old mice with the 2-way ANOVA (3 arms, 2 genotypes) revealed a significant arm effect ($F_{2,56}$ = 11.945, P < 0.0001), no effect of genotype nor of interaction between these 2 factors (see Fig. A in Supplemental Data). It was interesting to note that the mice preferred on the one hand the arm near the cue, as well as the starting arm, in comparison with the supposed neutral third arm. In addition, an unpaired T-test carried out on the cued arm revealed that the preference for this arm was significantly higher in the HeCo than in the control mice at P20 (P = 0.0210).

Figure B of the supplemental data illustrates the performance during task acquisition in the automated radial maze based on the number of visits in non baited arms (reference errors) until the mice had visited the 3 baited arms. The 2-way repeated measure ANOVA (genotype × 3-trials blocks) con-

ducted on the 2-month-old group revealed a significant effect of the repetition ($F_{2,25}$ = 20.375, P < 0.0001) and genotype ($F_{1,25}$ = 4.285, P = 0.0489) indicating better performance in controls but no interaction between genotype and repetition. The same analysis conducted in the groups aged above 7 months revealed also a significant effect of repetition ($F_{2,67}$ = 96.783, P < 0.0001) and genotype ($F_{1,67}$ = 7.655, P = 0.0073) without interaction but in this case results of control mice were worse.

During the Morris water maze task, the acquisition of spatial learning was assessed from the average number of errors (failures) in reaching the platform (see Fig. 10*A,B*). Separate 2-way repeated measure ANOVAs (genotype × days) were conducted as an indication of task acquisition in each age groups. There was a significant effect of genotype in the 7-month-old group ($F_{4,22}$ = 5.967, P = 0.0231), but not in the 2-month-old group. Indeed, the HeCo mice aged above 7 months were significantly impaired. A 2-way repeated measure ANOVA (age × days) revealed a significant effect of age ($F_{1,12}$ = 6.155, P = 0.0289) in the HeCo mice but not in the control group.

For the Probe trial, a 2-way measure ANOVA (genotype × age) on the bias toward the training position (i.e., % time in the reinforced half of the pool) during the probe trial did not reveal a significant effect (see Fig. 10*C*). However, a 2-way measure ANOVA (genotype × age) on the velocity during the probe trial (see Fig. 10*D*) revealed a significant effect of genotype ($F_{1,18}$ = 19.776, P = 0.0003) and of age ($F_{1,18}$ = 34.996, P < 0.0001).

In summary, when compared with controls, HeCo mice do not differ in overall growth rate, but show a significant delay in
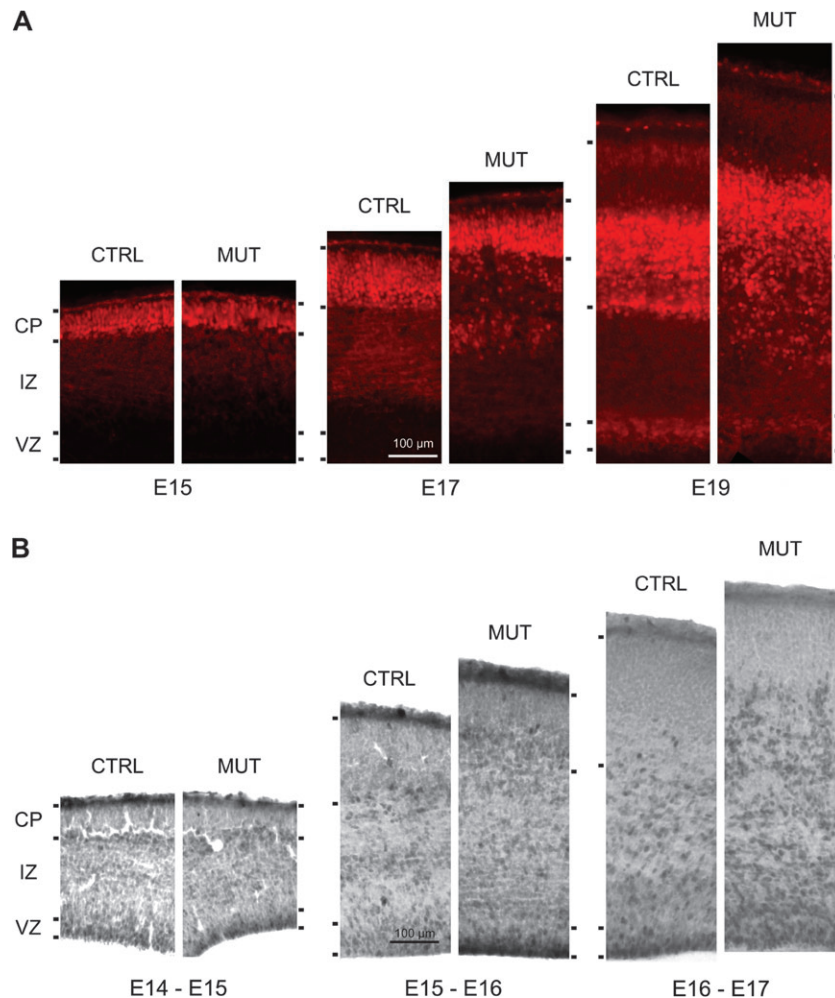
A

B

Figure 6. (*A*) Photomicrographs of coronal sections processed for Tbr-1 immunochemistry through the developing cerebral cortex of control (CTRL) and mutant (MUT) mice at embryonic age 15 (E15), 17 (E17), and 19 (E19). Note the thickness increase of the developing cortex in HeCo animals from E17, the cortical plate being more superficial. This was mainly due to an increase in thickness of the IZ. Note also the more diffuse distribution of Tbr-1 positive cells in HeCo animals at E17 and E19, some of them straggling within the IZ. (*B*) Photomicrographs of coronal sections processed for BrdU immunochemistry through the developing cerebral cortex of control (CTRL) and mutant (MUT) mice at embryonic age 15 (E15, BrdU injection at E14), 16 (E16, BrdU injection at E15), and 17 (E17, BrdU injection at E16). These images also show the increased thickness of the IZ and the corresponding larger extent of BrdU-positive cells within the IZ in HeCo animals at E16 and E17.

hair growth and eye opening, a slower development of loco-motion and a decrease in general activity as assessed by the Y-Maze task. They have a significantly lower performance during task acquisition in the automated radial maze and make significantly more errors in reaching the platform during the Morris water maze task at the age of 7 months.

Discussion

Human neuronal migration disorders are not uncommon pathologies, especially among epileptic patients (Meencke and Veith 1992; Guerrini 2005). Despite the discovery of the doublecortin gene, associated with the majority of cases of subcortical band heterotopia in humans (des Portes et al. 1998) and our current understanding of the mechanisms leading to cortical heterotopias (Clark 2004; Gressens 2006), a complete appreciation of the molecular and cellular events that underlie their pathogenesis is still needed. Different molecular pathways have been determined as important for neuronal migration, some involving the migrating neuron, others being necessary for correct interactions with glia and/or other neurons. Several

molecules of the cytoskeleton, or their associated proteins, have been shown to be involved in the migration of cortical neurons (Gressens 2006). In humans, filamin-A, an actin-binding protein, is mutated in periventricular nodular hetero-topia, Dcx, a microtubule-associated protein, is mutated in diffuse subcortical band heterotopia (double cortex) and lissencephaly, and Lis1, a microtubule-associated protein and dynein regulator, is mutated in isolated type 1 lissencephaly and Miller–Dieker syndrome (Gressens 2006). On the other hand, molecules of the reelin pathway, a glycoprotein mutated in lissencephaly associated with cerebellar hypoplasia in humans and in the reeler mouse mutant, are involved in cortical lamination (Gressens 2006). The molecules mentioned above are currently thought to be responsible for only a small percentage of the genetic disorders leading to the altered migration of cortical neurons in humans (Browne and Holmes 2001). To further develop the understanding of these neuronal migration disorders a larger number of animal models are therefore needed. Dcx null mutations in mice neither disrupt isocortical neuronal migration nor cause subcortical band heterotopia formation. In utero RNA interference of Dcx in
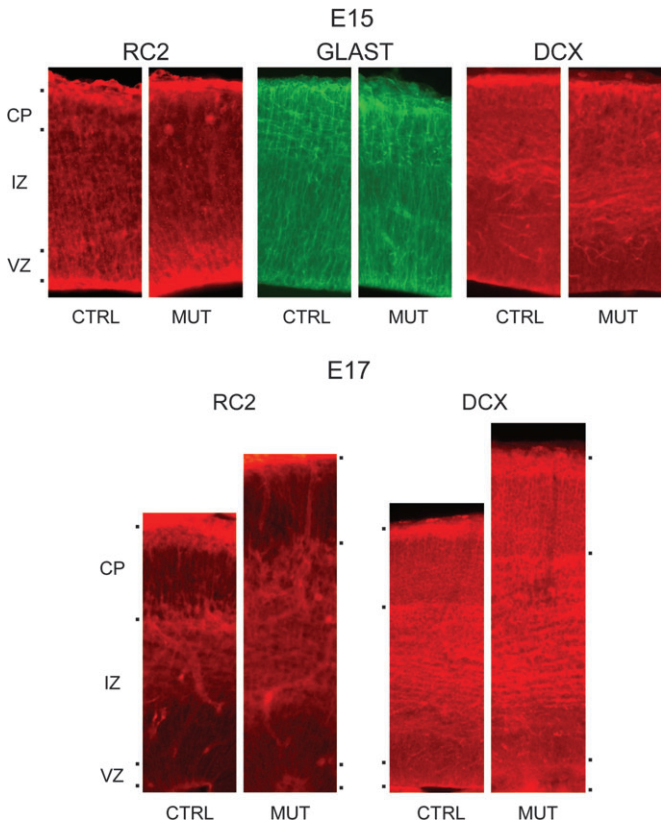
Figure 7. Photomicrographs of coronal sections processed for RC2, GLAST, and Dcx immunochemistry through the developing cerebral cortex of control (CTRL) and mutant (MUT) mice at embryonic age 15 (E15) and 17 (E17). Note again the increase in IZ thickness at E17 and the relatively similar pattern of labeling in both HeCo and control mice.

rats (but not in mice), in contrast, creates an animal model of subcortical band heterotopia (Corbo et al. 2002; Bai et al. 2003; Ramos et al. 2006). Other animal models of cortical malforma-

tions are the reeler mouse, the Lis1 knockout mouse and the spontaneous tish (telencephalic internal structural heterotopia) mutant rat (for review see Ross 2002). The tish rat is a spontaneous mutant that appeared in a colony of Sprague–Dawley rats (Lee et al. 1997). The transmission mode is autosomal recessive. Some of the affected animals present both electrographical and clinical seizures. In this mutant it was shown that the heterotopic neurons have connections with both the overlying cortex and deep structures such as the thalamic nuclei (Schottler et al. 1998), as in our model. It was proposed that, in the tish model, the abnormal band of gray matter is generated by an "extra" germinal zone (Lee et al. 1998) during preplate formation (E15). Therefore, the pathogenesis of the tish mutant occurs early during cortical development. Furthermore, the number of PARV+ neurons is decreased in tish rat normotopic and HeCo as compared with control animals and the PARV+ neurons within the HeCo are distributed in patches rather than in distinct layers as in control cortex (Trotter et al. 2006).

In our model however, the cells forming the heterotopia in the adult seem to be born mainly late in development. At P13, a moment where cortical layering is well established, the heterotopia is populated by neurons born at E18, an age that is well beyond the formation of the cortical plate and when the formation of the infragranular layers is already well underway. Furthermore, the results of the morphometric analysis concerning layer thickness, and cell density and size show that the superficial layers of the HoCo, normally populated by neurons born at E17-E18, displayed a decreased thickness and cell density compared with control animals. We also demonstrate that some of the neurons which have their final destination in the infragranular layers and which are born between E13 and E15 display an abnormal migration pattern because a condensed cell layer is already observed in the IZ at E16. However, at P13 these neurons have reached their correct position in the HoCo. The presence of PARV+ neurons within the HeCo together with the abnormal development of supragranular layers within the HoCo and AdCo further suggest that both projection and
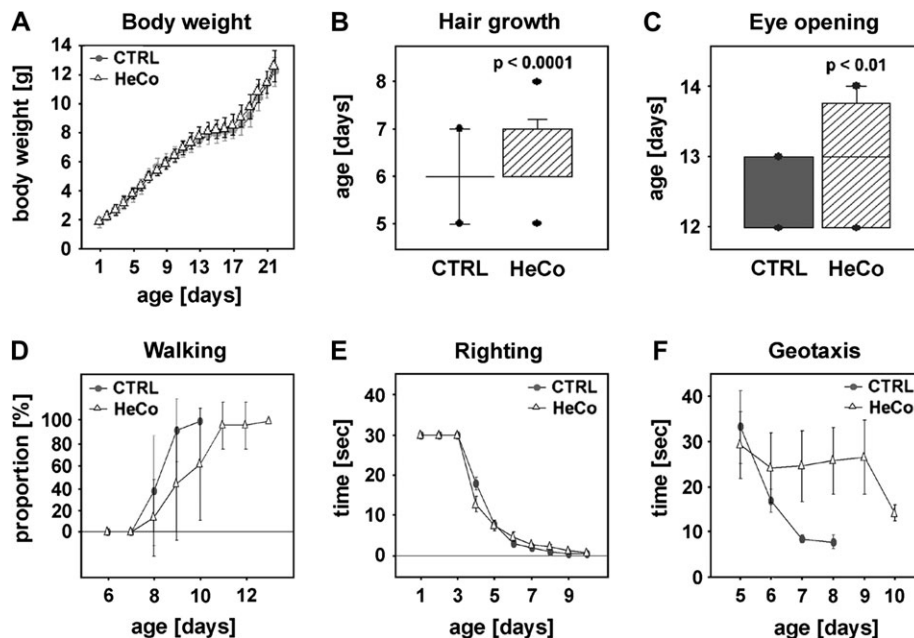

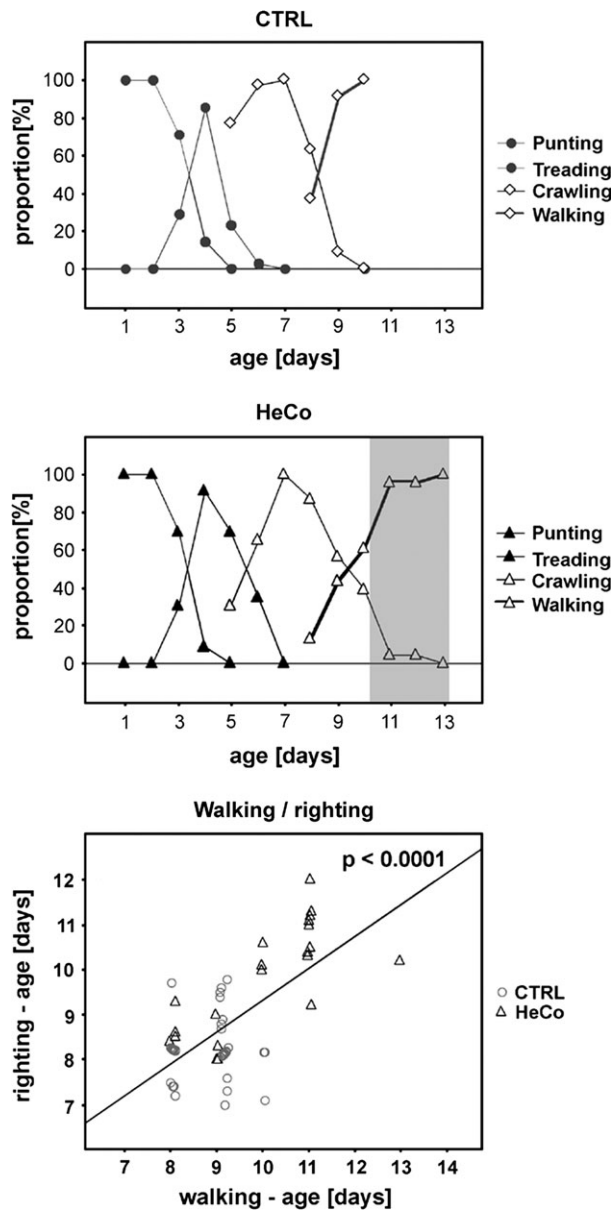**Figure 8.** Somatic growth. For details, see text.

Figure 9. Development of movement. Note that the development of the walk is delayed in HeCo mice and the correlation between the righting test and the apparition of walking. The gray stripe in the middle graph highlights the delay in the development of walking between control and HeCo mice. For details, see text.

interneuron migratory pathways in the forebrain are affected by the mutation.

The detailed comparison between the tish rat and HeCo indicates that cortical band heterotopia in these 2 animal models could be due to different molecular mechanisms. Therefore, the shared morphological and physiological features of the HeCo mouse and the tish rat do not imply necessarily that the mutated gene is identical in both models. To our knowledge the gene responsible for the cortical malformation in tish rat has not yet been identified. We are currently localizing the gene mutation in the HeCo genome using polymorphic marker analyses as part of an ongoing collaboration with the Institut Cochin, France and the French Centre National de Génotypage.

Recently, LoTurco and Bai (2006) hypothesized that the perturbation of early phases of cortical development (e.g., after

loss of filamin-A function), creates nodular periventricular heterotopia because cells remain in the so-called multipolar stage and are unable to polarize and make radial progress through the IZ. By contrast, they hypothesized that failure or delay of the transition out of the multipolar stage, for instance in the case of Dcx or LIS1 mutations, could cause formation of subcortical band heterotopia. The HeCo phenotype seems to be comparable with this second type of subcortical band formation as was shown notably by the birth date analyses and the increase in IZ thickness visualized using the anti-Tbr-1 antibody. Interestingly, when we observe the first signs of HeCo formation, markers of radial glia (RC2 and GLAST), as well as Dcx, display a pattern that is roughly similar to that in control mice.

The tendency to develop epilepsy in the tish rat was linked to a disturbance of inhibitory GABAergic neurotransmission before seizure onset, characterized by an altered GABAergic neuron distribution in both heterotopic and normotopic cortex, and a significant reduction in the frequency and amplitude of spontaneous inhibitory postsynaptic currents (sIPSCs) and miniature inhibitory postsynaptic currents (IPSC) recorded from pyramidal neurons (Trotter et al. 2006). Interestingly, the amplitudes of sIPSCs in normotopic cortex were also reduced. In human patients suffering from periventricular nodular heterotopia, interictal spiking activity was found in ectopic gray matter but also in the cortex overlying the nodules and in the mesial temporal structures. The heterotopia was involved in seizure onset in the majority of patients, but some patients had seizures originating in mesial temporal structures only (Aghakhani et al. 2005). We demonstrate here that the density of PARV+ neurons in the HeCo is of the same magnitude as in the overlying HoCo, and as in control cortex. We realize that the density of PARV+ neurons is just one parameter characterizing the GABAergic system, roughly representing 50% of the normal number of GABAergic neurons in cerebral cortex. In addition to such a number, more information is needed on the synaptology of GABAergic innervation of the HeCo, as well as the mode of transmission within this part of the nervous system before a possible link could be proposed on the origin of the lowered threshold for epileptogenesis in the HeCo mouse.

The results of the behavioral experiments indicate a significantly delayed somatic maturation (eye opening and fur growing) in the HeCo mice. This was accompanied by delays in the maturation of locomotor abilities, particularly in the geotaxis response. No genotype effect was evident in the expression of spontaneous alternation in juvenile subjects, but HeCo mice expressed a more marked preference for the cued arm at the age of 20 days, suggesting a marked tendency in cue guidance (see Wiener and Schenk 2005). In the adult subjects the cognitive performance was nearly normal in HeCo mice at the age of 2 months. In the radial maze in particular, it is possible that a cue guidance might have facilitated an optimal performance because the task design required only reference memory capacities. This suggests that HeCo mice were dependent on olfactory or visuo-spatial cues for spatial performance. Thus, HeCo mice appeared more adaptive, selecting the specific cues in comparison with control mice. During the Morris water maze task, no effect of genotype in the 2-month-old group was observed, indicating relatively preserved memory abilities in young animals. This conclusion is in accordance with the results of the neuropsychological assessment reported in children with subcortical band heterotopia due to a mutation
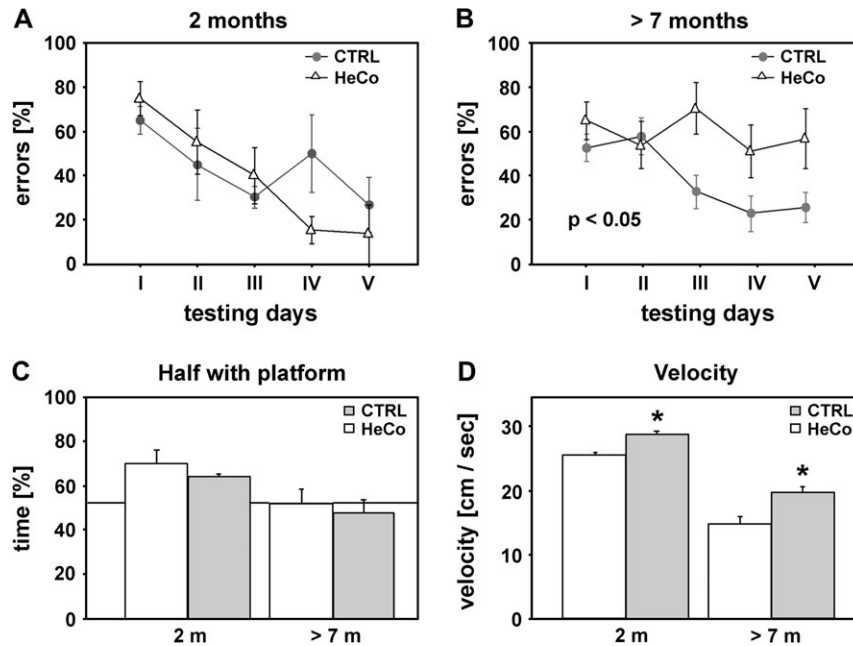
Figure 10. Morris water maze task. (*A* and *B*) Average number of errors during acquisition. (*C* and *D*) Probe trial on day 5. (*C*) Mean (±SE) time spent in the half containing the platform. At 2 months all animals showed a significant bias toward the quadrant containing the platform. (*D*) Speed during a 60-s exploration. HeCo mice were significantly slower than control mice. Asterisks highlight statistical significance.

in Dcx, which demonstrated intellectual impairment and deficits in all cognitive domains (processing speed, attention, language, visuomotor skills and fine motor ability) except verbal and visual episodic memory (Hashimoto et al. 1993; Jacobs et al. 2001; D'Agostino et al. 2002; Janzen et al. 2004).

We present here a new and unique mouse model of cortical heterotopia. This model shares with its human counterpart the morphology of the HeCo which lies inside the subcortical white matter, a certain degree of ventricular enlargement, the presence of GABA cells inside the HeCo (Hammers et al. 2001), and a tendency to develop epileptic seizures and SE (Meencke and Veith 1992). It represents therefore a true animal model of cortical heterotopia. The difference in transmission mode (X-linked for human "double cortex," autosomal recessive for the HeCo mouse), suggests that the gene involved here is part of a new, as yet uncharacterized pathway, and cloning this gene will undoubtedly contribute to our understanding of cerebral cortex development.

Furthermore, the presence of spontaneous epileptic seizures, at least in the younger animals, makes this model a useful tool to study spontaneous chronic epilepsy in the mouse and to examine the relationship between structural abnormalities and epileptogenesis as well as structural modifications after epileptic seizures. It is also likely to provide a new tool to test and develop antiepileptic therapies.

Supplementary Material

Supplementary material can be found at: http://www.cercor.oxfordjournals.org/

Address correspondence to Alexandre Croquelois, MD, Service de Neuropsychologie et de Neuroréhabilitation, Unité Universitaire de Neuroréhabilitation, Centre Hospitalier Universitaire Vaudois (CHUV), Avenue Pierre Decker 5, CH-1011 Lausanne, Switzerland. Email: alexandre.croquelois@chuv.ch.

References

Aghakhani Y, Kinay D, Gotman J, Soualmi L, Andermann F, Olivier A, Dubeau F. 2005. The role of periventricular nodular heterotopia in epileptogenesis. Brain. 128:641-651.

Altman J, Sudarshan K. 1975. Postnatal development of locomotion in the laboratory rat. Anim Behav. 23:896-920.

Bai J, Ramos RL, Ackman JB, Thomas AM, Lee RV, LoTurco JJ. 2003. RNAi reveals doublecortin is required for radial migration in rat neocortex. Nat Neurosci. 6:1277-1283.

Browne TR, Holmes GL. 2001. Epilepsy. N Engl J Med. 344:1145-1151.

Cavalheiro EA, Santos NF, Priel MR. 1996. The pilocarpine model of epilepsy in mice. Epilepsia. 37:1015-1019.

Clark GD. 2004. The classification of cortical dysplasias through molecular genetics. Brain Dev. 26:351-362.

Corbo JC, Deuel TA, Long JM, LaPorte P, Tsai E, Wynshaw-Boris A, Walsh CA. 2002. Doublecortin is required in mice for lamination of the hippocampus but not the neocortex. J Neurosci. 22:7548-7557.

Croquelois A, Bronchti G, Welker E. 2005. Cortical origin of functional recovery in the somatosensory cortex of the adult mouse after thalamic lesion. Eur J Neurosci. 21:1798-1806.

D'Agostino MD, Bernasconi A, Das S, Bastos A, Valerio RM, Palmini A, Costa da CJ, Scheffer IE, Berkovic S, Guerrini R, et al. 2002.

Subcortical band heterotopia (SBH) in males: clinical, imaging and genetic findings in comparison with females. Brain. 125:2507-2522.

des Portes V, Pinard JM, Billuart P, Vinet MC, Koulakoff A, Carrie A, Gelot A, Dupuis E, Motte J, Berwald-Netter Y, et al. 1998. A novel CNS gene required for neuronal migration and involved in X-linked subcortical laminar heterotopia and lissencephaly syndrome. Cell. 92:51-61.

Dobyns WB, Truwit CL. 1995. Lissencephaly and other malformations of cortical development: 1995 update. Neuropediatrics. 26:132-147.

Eriksson SH, Malmgren K, Nordborg C. 2005. Microdysgenesis in epilepsy. Acta Neurol Scand. 111:279-290.

Farrell MA, DeRosa MJ, Curran JG, Secor DL, Cornford ME, Comair YG, Peacock WJ, Shields WD, Vinters HV. 1992. Neuropathologic findings in cortical resections (including hemispherectomies) performed for the treatment of intractable childhood epilepsy. Acta Neuropathol. 83:246-259.

Grandchamp N, Schenk F. 2006. Adaptive changes in a radial maze task: efficient selection of baited arms with reduced foraging in senescent hooded rats. Behav Brain Res. 168:161-166.

Gressens P. 2000. Mechanisms and disturbances of neuronal migration. Pediatr Res. 48:725-730.

Gressens P. 2006. Pathogenesis of migration disorders. Curr Opin Neurol. 19:135-140.

Guerrini R. 2005. Genetic malformations of the cerebral cortex and epilepsy. Epilepsia. 46(Suppl 1):32-37.

Hammers A, Koepp MJ, Richardson MP, Labbe C, Brooks DJ, Cunningham VJ, Duncan JS. 2001. Central benzodiazepine receptors in malformations of cortical development: a quantitative study. Brain. 124:1555-1565.

Hashimoto R, Seki T, Takuma Y, Suzuki N. 1993. The 'double cortex' syndrome on MRI. Brain Dev. 15:57-59.

Honda T, Tabata H, Nakajima K. 2003. Cellular and molecular mechanisms of neuronal migration in neocortical development. Semin Cell Dev Biol. 14:169-174.

Jacobs R, Anderson V, Harvey AS. 2001. Neuropsychological profile of a 9-year-old child with subcortical band heterotopia or 'double cortex'. Dev Med Child Neurol. 43:628-633.

Janzen L, Sherman E, Langfitt J, Berg M, Connolly M. 2004. Preserved episodic memory in subcortical band heterotopia. Epilepsia. 45:555-558.

Lee KS, Collins JL, Anzivino MJ, Frankel EA, Schottler F. 1998. Heterotopic neurogenesis in a rat with cortical heterotopia. J Neurosci. 18: 9365-9375.

Lee KS, Schottler F, Collins JL, Lanzino G, Couture D, Rao A, Hiramatsu K, Goto Y, Hong SC, Caner H, et al. 1997. A genetic animal model of human neocortical heterotopia associated with seizures. J Neurosci. 17:6236-6242.

LoTurco JJ, Bai J. 2006. The multipolar stage and disruptions in neuronal migration. Trends Neurosci. 29:407-413.

Meencke HJ, Veith G. 1992. Migration disturbances in epilepsy. Epilepsy Res Suppl. 9:31-39.

Meencke HJ, Veith G. 1999. The relevance of slight migrational disturbances (microdysgenesis) to the etiology of the epilepsies. Adv Neurol. 79:123-131.

Rakic P. 1988. Defects of neuronal migration and the pathogenesis of cortical malformations. Prog Brain Res. 73:15-37.

Rakic P. 2003. Elusive radial glial cells: historical and evolutionary perspective. Glia. 43:19-32.

Ramos RL, Bai J, LoTurco JJ. 2006. Heterotopia formation in rat but not mouse neocortex after RNA interference knockdown of DCX. Cereb Cortex. 16:1323-1331.

Ross ME. 2002. Brain malformations, epilepsy, and infantile spasms. Int Rev Neurobiol. 49:333-352.

Schottler F, Couture D, Rao A, Kahn H, Lee KS. 1998. Subcortical connections of normotopic and heterotopic neurons in sensory and motor cortices of the tish mutant rat. J Comp Neurol. 395:29-42.

Takahashi T, Nowakowski RS, Caviness VS, Jr. 1992. BUdR as an S-phase marker for quantitative studies of cytokinetic behaviour in the murine cerebral ventricular zone. J Neurocytol. 21:185-197.

Trotter SA, Kapur J, Anzivino MJ, Lee KS. 2006. GABAergic synaptic inhibition is reduced before seizure onset in a genetic model of cortical malformation. J Neurosci. 26:10756-10767.

Van der Loos H, Welker E, Dorfl J, Rumo G. 1986. Selective breeding for variations in patterns of mystacial vibrissae of mice. Bilaterally symmetrical strains derived from ICR stock. J Hered. 77:66-82.

Veenman CL, Reiner A, Honig MG. 1992. Biotinylated dextran amine as an anterograde tracer for single- and double-labeling studies. J Neurosci Methods. 41:239-254.

Wiener SI, Schenk F. 2005. Behavioral studies of directional orientation in developing and adult animals. In: Taube JS, Wiener SI, editors. Head direction cells and the neural mechanisms underlying directional orientation. Cambridge: Massachusetts Institute of Technology Press. p. 247-274.

Wonders C, Anderson SA. 2005. Cortical interneurons and their origins. Neuroscientist. 11:199-205.